Structural Engineering and Mechanics, *Vol. 53, No. 5 (2015) 897-919*
DOI: http://dx.doi.org/10.12989/sem.2015.53.5.897

Multi-point response spectrum analysis of a historical bridge to blast ground motion

Kemal Hacıefendioğlu[*1], Swagata Banerjee[2a], Kurtuluş Soyluk[3b] and Olgun Köksal[4c]

[1]*Department of Civil Engineering, Ondokuz Mayıs University, 55139, Samsun, Turkey*
[2]*Department of Civil and Environmental Engineering,The Pennsylvania State University, 16802-1408, USA*
[3]*Department of Civil Engineering, Gazi University, Maltepe, 06570 Ankara, Turkey*
[4]*Vocational High School of Kavak, Ondokuz Mayıs University, 55139, Samsun, Turkey*

(Received February 28, 2014, Revised October 10, 2014, Accepted October 28, 2014)

Abstract. In this study, the effects of ground shocks due to explosive loads on the dynamic response of historical masonry bridges are investigated by using the multi-point shock response spectrum method. With this purpose, different charge weights and distances from the charge center are considered for the analyses of a masonry bridge and depending on these parameters frequency-varying shock spectra are determined and applied to each support of the two-span masonry bridge. The net blast induced ground motion consists of air-induced and direct-induced ground motions. Acceleration time histories of blast induced ground motions are obtained depending on a deterministic shape function and a stationary process. Shock response spectrums determined from the ground shock time histories are simulated using BlastGM software. The results obtained from uniform and multi-point response spectrum analyses cases show that significant differences take place between the uniform and multi-point blast-induced ground motions.

Keywords: historic masonry bridge; blast-induced ground motion; multi-point response spectrum method; charge weight; charge center

1. Introduction

Turkey is one of the richest countries in the world in terms of historical monuments. Most of these monuments are located in Balkans, Middle East and North Africa which constitute a part of the cultural heritage of the Ottoman Empire and serve today as a bridge between Turkey and the countries concerned (Url-1 2014). Historical monuments playing an important role in the reflection of the most priceless cultural heritage and identity create a strong bond between the past and today. With this regard there are plenty of masonry bridges in Anatolia, Turkey and approximately 1300 of these historical bridges are still in-service. The first of these bridges were built during the Hittite period, and followed by the construction during the Ottoman period. These historic bridges, especially the ones constructed in the 19 century during the Ottoman period, are

∗Corresponding author, Associate Professor, E-mail: hckemal@omu.edu.tr
[a]Assistant Professor, E-mail: swagata@engr.psu.edu
[b]Professor, E-mail: ksoyluk@gazi.edu.tr
[c]Teaching Assistant, E-mail: olgun.koksal@omu.edu.tr

http://www.techno-press.org/?journal=sem&subpage=8 ISSN: 1225-4568 (Print), 1598-6217 (Online)

usually single span stone arch bridges (Ural *et al*. 2008).

Dynamic behavior of these historical structures should also be determined under heavy explosions due to the explosive, gunpowder, gasoline, chemical reactions, etc. for their protection and restoration. It is possible to investigate the dynamic behavior of most of these structures in a realistic way with the finite element method by modeling the bridges as having curvilinear geometric form with stone and brick masonry.

Studies related to the static and dynamic behavior of masonry arch bridges have been conducted recently. Toker and Unay (2004) showed the mathematical modeling techniques on a prototype model of a common arch bridge under different loading conditions. Ural (2005) carried out the seismic analysis of Cosandere Historical Arch Bridge subjected to El-Centro ground motion record. Bayraktar *et al*. (2007) determined the dynamic characteristics of Historical Sinik Bridge under ambient vibrations. Bhatti (2009) investigated the seismic vulnerability of arch type masonry bridge structures which were designed primarily for gravity loads. Pelà *et al*. (2009) evaluated the seismic performance of existing masonry arch bridges by using nonlinear static analysis, as suggested by several modern standards such as UNI ENV 1998-1 2003, OPCM 3274 2004, and FEMA 440 2005. Sevim *et al*. (2011) determined the importance of model calibration and in situ vibration testing of two historical arch bridges by comparing the finite element model predictions of earthquake responses of these bridges before and after model calibration. Sayın *et al*. (2011) studied the linear and non-linear dynamic seismic analyses of Uzunok Bridge in the town center of Darende of Malatya City. The historical bridge was modeled by three-dimensional finite element model and the results obtained from the linear and non-linear solutions were compared with each other. Gonen *et al*. (2013) illustrated the deformations and stresses of Murat Masonry Arch Bridge in Turkey under dead load as well as earthquake load.

So far, many historical bridges have been exposed to natural disasters such as earthquakes, floods, and high winds and accordingly they have been damaged or destroyed. In addition to these effects, historical bridges have been gradually disappeared due the loss of the strength of the materials and uneven loadings such as blast loading. Surface explosion is one of the potential environmental threats like earthquake and wind for historical structures and can cause partly or completely damage on nearby structures. Therefore, historical structures have to resist these kinds of loads during their entire life period (Hacıefendioğlu *et al*. 2013, Haciefendioglu and Alpaslan 2014). For this purpose, blast type loading should be included in the analysis and restoration design of historical structures to minimize the cracks or any kind of damages.

The influence of blast loading on historical structures depend primarily on vibration levels, excitation frequencies, site conditions, distances from the blast's source and structural properties. This type of a load generates ground vibrations and air blast pressures on nearby structures. The generated ground vibrations reach to the foundations of the structure before the air blast pressure. Therefore, before investigating the total effect caused by blast type loading on structures, emphasizing the importance of the blast-induced ground motion can be more expressive for the dynamic response analysis of structural systems. Very limited research has been conducted so far about the blast-induced ground motions (Wu *et al*. 2004, Ma *et al*. 2004, Hao and Wu 2005, Lu and Wang 2006, Wu and Hao 2005, Wu and Hao 2007, Singh and Roy 2010, Hacıefendioğlu *et al*. 2012, Hacıefendioğlu and Alpaslan 2014).

Previous studies revealed that spatial variability of both the seismic and blast induced ground motions strongly affects the structural responses (Downding 1996, Hao 1989). Spatial variation of the blast induced ground motion is more evident thanthose of the seismic ground motion due to the close distance of the structure from the source center. Spatial variability properties of blast induced ground motions are important in order to be able to assess its effects on structures more accurately. Unfortunately, only few studies were conducted about the effects of spatial variability of blast induced ground motions (Hao *et al*. 2001, Mclaughlin *et al*. 1983, Reinke and Stump 1988, Todo and Dowding 1984).

It seems that previous studies are mainly focused on the seismic earthquake response analyses of historical masonry bridges. Therefore, in this study it is intended to carry out a three-dimensional dynamic analysis of a masonry historical bridge subjected to blast-induced ground motion by using the multi-point response spectrum method. ANSYS (2013) is utilized to perform the required numerical calculations of dynamic analysis. For numerical calculations, three different charge weights with three different charge centers are used and shaded image contours and spectral responses of the masonry bridge are determined.

2. Finite element formulation of multi-point ground motion

The effect of multi-support seismic ground motion on large structures has been investigated by many researchers. These studies revealed that the dynamic response of large structures under multi-support seismic ground motion is different from those of the uniform ground motion. However, multi-support seismic ground motion may be neglected for small structures such as elevated fluid tanks, towers and multi-stored buildings due to the fact that horizontal-longitudinal structural dimensions of these structures are often small with respect to the seismic wave lengths. Because of the epicentral distance from the explosion center, blast-induced ground motions normally have very high frequency contents that cause it varying drastically over a short propagation distance. Spatial variation of blast induced ground motions becomes more significant in order to more accurately assess its effects on structures which are not large unlike strong ground motions caused by earthquakes (Hiroki and Charles 1984, Hao *et al*. 2001, Wu and Hao 2005). All studies related to the spatial variation of the blast induced ground motions revealed the significant influence of random geologic conditions on near field stress waves. Because of the high frequency content and rapid attenuation, spatial variability effect for the near field blast induced ground motion is more evident than those of the earthquake ground motion (Hao *et al*. 2001, Mclaughlin 1983, Reinke and Stump 1988). Due to the lack of suitable ground motion models for the spatial variability of multi-point blast induced ground motions, the spatially varying ground motion components of wave passage and incoherent effects are not considered in this study. The spatial variability effect of the blast-induced ground motion is considered with the response spectrum curves having peak accelerations sensitive to the distance from blast center and soil condition. Peak acceleration values are calculated using the equations determined from the parametrical and experimental studies (Wu and Hao 2004, UFC 2008, Wu and Hao 2007) where the effects of wave velocity in the soil or on the soil surface and characteristic soil properties are considered for the propagation of the explosion.

The dynamic equations of motion of a structure discretized using the finite element method may be written in the partitioned form (Harichandran *et al*. 1996, Harichandran and Wang 1990)

$$\begin{bmatrix} M_{rr} & M_{rg} \\ M_{gr} & M_{gg} \end{bmatrix} \begin{Bmatrix} \ddot{u}_r \\ \ddot{u}_g \end{Bmatrix} + \begin{bmatrix} C_{rr} & C_{rg} \\ C_{gr} & C_{gg} \end{bmatrix} \begin{Bmatrix} \dot{u}_r \\ \dot{u}_g \end{Bmatrix} + \begin{bmatrix} K_{rr} & K_{rg} \\ K_{gr} & K_{gg} \end{bmatrix} \begin{Bmatrix} u_r \\ u_g \end{Bmatrix} = \begin{Bmatrix} 0 \\ 0 \end{Bmatrix} \tag{1}$$

where [M], [C], [K] are the mass, damping and stiffness matrices, respectively; $\{\ddot{u}\}, \{\dot{u}\}, \{u\}$ are the vectors of total acceleration, velocity and displacement, respectively. The subscript *r* denotes the structural degrees of freedom and *g* denotes the ground degrees of freedom. It is possible to separate the total displacement vector as quasi-static and dynamic parts as follows

$$\{u_r\} = \{u_{sr}\} + \{u_{dr}\} \tag{2}$$

Structural quasi-static displacements may be obtained from Eq. (1) by eliminating the first two terms on the left-hand side of the equation.

$$\{u_{sr}\} = -[K_{rr}]^{-1}[K_{rg}]\{u_{sg}\} = [R_{rg}]\{u_{sg}\} \tag{3}$$

in which $[R_{rg}] = -[K_{rr}]^{-1}[K_{rg}]$. Substituting Eqs. (2) and (3) into Eq. (1), the equations of motion of the dynamic component of the structural degrees of freedom can be written as

$$[M_{rr}]\{\ddot{u}_{dr}\} + [C_{rr}]\{\dot{u}_{dr}\} + [K_{rr}]\{u_{dr}\} = -[M_{rr}][R_{rg}]\{\ddot{u}_{sg}\} \tag{4}$$

Using the well-known modal analysis approach and letting $\{u_{dr}\} = [\phi]\{Y\}$ decouples the above equations to yield

$$\ddot{Y}_i + 2\xi_i\omega_i\dot{Y}_i + \omega_i^2 Y_i = G_i \tag{5}$$

in which Y_i is the generalized displacement, ω_i and ξ_i are the natural frequencies and modal damping ratios, and $G_i = (\Gamma_i)^T\{\ddot{u}_g\}$ is the modal load. The modal participation factor is defined by

$$\{\Gamma_i\} = [M_{rr}][R_{rg}]\{\phi_i\} \tag{6}$$

2.1 Multi-point response spectrum method

Multi-point response spectrum method gives the possibility to assign different base boundaries to different response spectra. In this method, input spectrums are assumed to be uncorrelated with each other.

The participation factor, Γ_{il} , for the l^{th} input spectrum are computed by Eq. (6) and the mode coefficients for the l^{th}input spectrum are defined by

$$B_{il} = S_{il}.\Gamma_{il} \tag{7}$$

where S_{il} is the interpolated input response spectrum for the l^{th}input spectrum at the i^{th} natural frequency. The mode coefficients are combined using SRSS

$$A_i = \left(B_{i1}^2 + B_{i2}^2 + B_{i3}^2 + \cdots\right)^{\frac{1}{2}} \tag{8}$$

Once the maximum response at each mode is known for the given response spectrum, these modes are combined using variety of methods to get the total response of the structures. The displacement, velocity and acceleration responses for each mode may be computed from the frequency, mode coefficient and mode shape as follows

$$\{R\}_i = A_i.\{\phi\}_i \rightarrow \text{for displacement response}$$

$$\{R\}_i = \omega_i A_i.\{\phi\}_i \rightarrow \text{for velocity response}$$

$$\{R\}_i = \omega_i^2 A_i.\{\phi\}_i \rightarrow \text{for acceleration response} \tag{9}$$

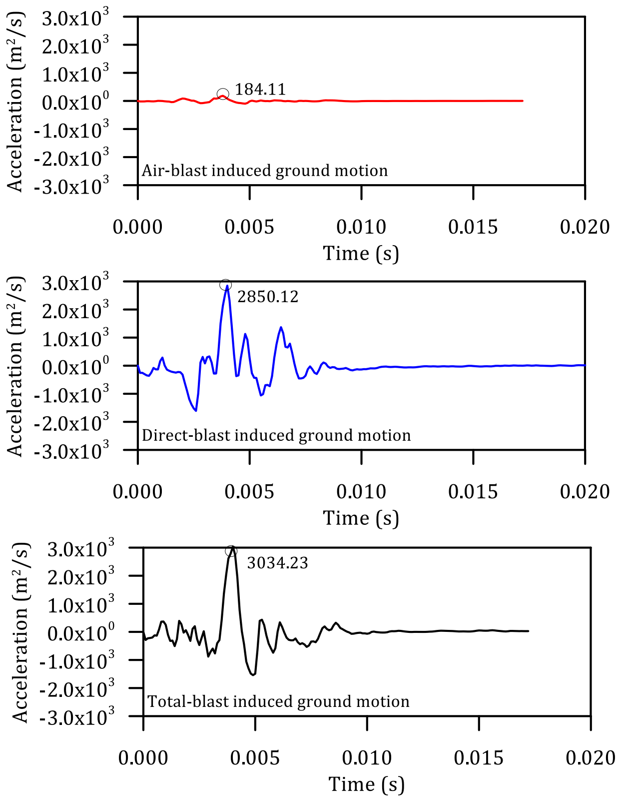

Fig. 1 Time histories of air, direct and total blast induced ground motions due to 1250 kg charge weight and 10 m blast distance (Köksal 2013)

For each input spectrum, mode shapes, mode stresses, etc. are multiplied by mode coefficients to compute the modal quantities, which are then combined with the available mode combination techniques (SRSS, CQC, Double Sum, Grouping, NRL-SUM or Rosenblueth method). In this study, structural responses are determined using the SRSS method from each spectrum (Gupta 1992).

3. Blast-induced random ground motion models

In this part of the paper, the effect of ground-shock caused by accidental explosions on structures and their contents are defined. As known, large amount of energy reveals due to the explosions. Some of this energy is transmitted through the air in the form of air-blast-induced ground shock and some is transmitted through the ground as direct-induced ground shock (if the charge is located on or beneath the surface of the soil) (UFC 2008). Air-induced ground shock occurs when the air blast shock wave compresses the ground surface and induces a stress impulse into the underlying media. Direct-induced ground shock results from the explosive energy being transmitted directly through the ground. The net (total) ground shock experienced is a combination of both (Tuma *et al*. 2011).The time histories of air, direct and total blast induced ground motions calculated by BlastGM computer program (Köksal 2013) are shown in Fig. 1.

The soil type, the air temperature, the density of the media through which the shock travels, and the distance from the blast center determine the effect of the ground shock. It is known that the effect of the air blast on a structure is larger than those of the ground shock. Previous studies have generally neglected the ground shock effect (direct-induced ground shock) for the dynamic analysis of aboveground structures. However, recently performed studies (Haciefendioglu *et al*. 2012, Haciefendioglu and Alpaslan 2014) have shown the importance of the ground shock effect.

3.1 Air-Blast induced ground shock

One-dimensional wave propagation theory is effectively used in estimating the air-blast induced ground shocks. The expressions related to the air-blast induced ground shock waves are given below (UFC 2008). The maximum horizontal ground motion accelerations depending on the maximum vertical motions are expressed as a function of the seismic velocity of the soil and the shock wave velocity

$$PPA_V = 1{,}200\, P_{so} / (\rho C_p g) \tag{10}$$

$$PPA_H = PPA_V \tan\left[\sin^{-1}\left(C_p / U\right)\right] \tag{11}$$

where PPA_V and PPA_H are the maximum vertical and horizontal accelerations of the ground surface, respectively, g is the gravitational constant equal to 9.81 m/sec^2, ρ is the mass density of the soil, C_p is the compressional seismic wave velocity in the soil and U is the shock front velocity which is obtained from Fig. 2. While the mass density, ρ, for typical soils and rock are presented in Table 1, the seismic wave velocities are presented in Table 2.

If $\tan\left[\sin^{-1}\left(C_p / U\right)\right] > 1$, horizontal and vertical motions will be approximately equal to each other.

Table 1 Mass densities for typical soils and rocks (UFC 2008)

Material	Mass Density, ρ (kg-sn^2)/m^4
Loose, dry sand	154.746
Loose, saturated sand	195.067
Dense, dry sand	179.810
Dense, saturated sand	220.132
Dry clay	122.053
Saturated clay	179.810
Dry, sandy silt	171.092
Saturated, sandy silt	212.503
Basalt	278.979
Granite	269.171
Limestone	245.196
Sandstone	228.850
Shale	236.478
Concrete	245.196

Table 2 Typical seismic velocities for soils and rocks (UFC 2008)

Material	Seismic Velocity (m/sec)
Loose and dry soils	182.880-1005.840
Clay and wet soils	762.000-1920.240
Coarse and compact soils	914.400-2590.800
Sandstone and cemented soils	914.400-4267.200
Shale and marl	1828.800-5334.000
Limestone-chalk	2133.600-6400.800
Metamorphic rocks	3048.000-6400.800
Volcanic rocks	3048.000-6858.000
Sound plutonic rocks	3962.400-7620.000
Jointed granite	243.840-4572.000
Weathered rocks	609.600-3048.000

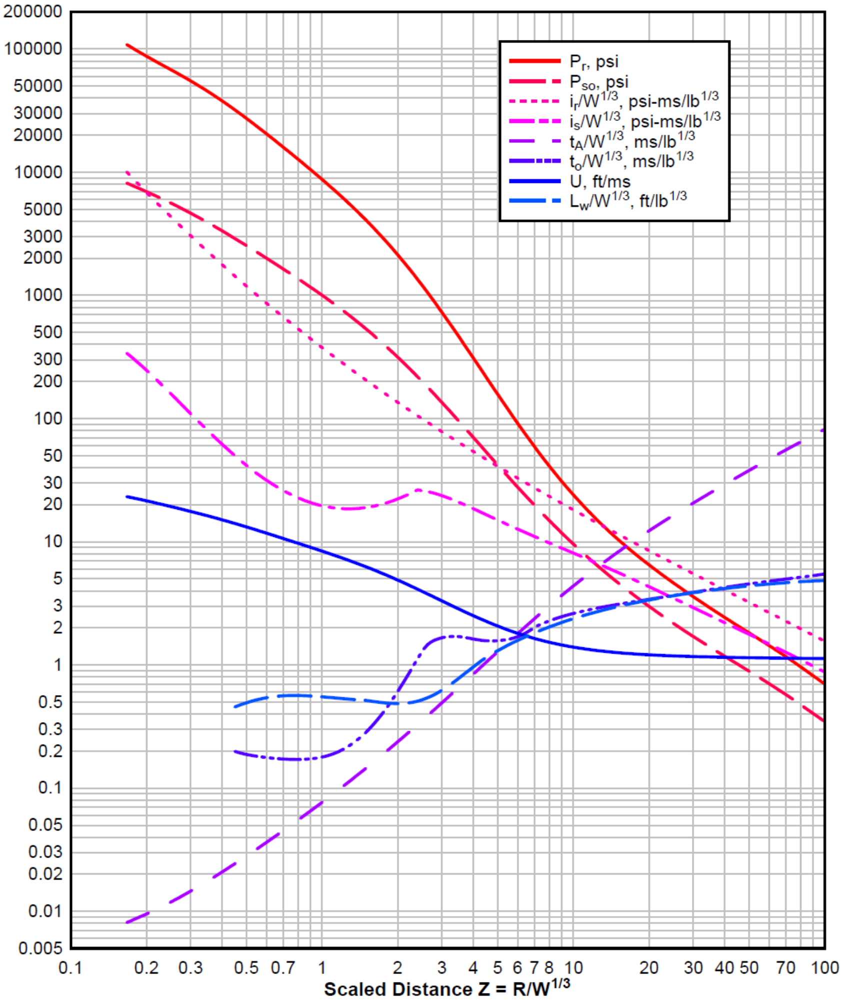

Fig. 2 Positive phase shock wave parameters for a hemispherical TNT explosion on the surface of sea level (UFC 2008)

3.2 Direct-induced ground shock

Direct-induced ground motions are determined from an empirical formula. These equations are used for TNT detonations at or near the ground surface. The charge weight and distance from the explosion are effective for the ground shock parameters. Maximum horizontal acceleration (PPA) of the ground surface for rock media is given by (Wu and Hao 2005)

$$PPA = 3.979 R^{-1.45} Q^{1.07} \quad (g) \tag{12}$$

where R is the distance in meters measured from the charge center and Q is the TNT charge weight in kilograms.

3.3 Generation of shock response spectrum

Ground motion time histories on a rock surface are simulated by using the above defined parameters. Blast-induced ground motion time histories including the effects of air blast induced and direct-induced ground shocks are obtained to determine the shock response spectrums which are then used to perform the dynamic analysis of the considered structure under multi-point blast induced ground motions. Due to the fact that it is difficult to obtain blast-induced ground shock time histories experimentally, BlastGM (Köksal 2013) software is used in this study to simulate shock response spectra arising from the ground shock time histories.

Non-stationary random process method is utilized to model the blast-induced ground motions. In this approach, ground motion acceleration values depending on time are obtained by using the parameters of a deterministic shape function of time (time intensity envelope function), p(t), and a stationary white noise, $w(t)$ of intensity S_0 (Bolotin 1960, Jennings *et al*. 1969, Ruiz and Penzien 1969). Non-stationary blast-induced ground motions can be obtained by using Eq. (13) as suggested by Amin and Ang (1968).

$$a_b(t) = p(t) w(t)_{sta} \tag{13}$$

A time intensity envelope function is used to calculate the non-stationary seismic ground motion in the time domain in earthquake engineering. The shape function $\eta(t)$ is obtained from the Hilbert transform (Kanasewich 1981). The envelope of the blast-induced ground motion can be appropriately modeled as an exponential function by using a shape function as defined by Eq. (14) (Wu and Hao 2004).

$$\eta(t) = \begin{cases} 0, & t \le 0, \\ mte^{-nt^2} & t > 0, \end{cases} \tag{14}$$

In this equation, terms m and n depend on the non-stationary ground motion and e is the base of the natural logarithm. The general shape function of a blast-induced ground motion is illustrated in Fig. (3)

In order to generate wave forms as a representative ground motion, the first step is to produce samples of white noise. Then, by using the shape function, they are shaped and passed through the filter. The generation of a sequence of independent random numbers u_j with uniform distribution in the interval (0, 1) is obtained. The derivation of a new sequence of independent random numbers w_j with Gaussian distributions having zero mean and unit variance is computed by leveraging Ruiz and Penzien study (1969).

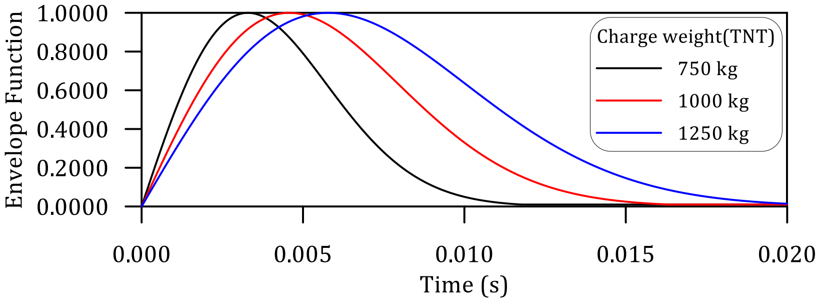

Fig. 3 The envelope function of total blast-induced ground motion

The wave forms of the bedrock acceleration are derived from second order differential equation as shown in Eq. (15).

$$\begin{aligned} &\ddot{u} + 2\zeta\omega_0\dot{u} + \omega_0 u = -a_b(t) \\ &a_g(t) = -2\zeta\omega_0\dot{u} + \omega_0^2 u \end{aligned} \tag{15}$$

Shock response spectrum is a calculated function based on the peak value (maximum or minimum) of the ground shock acceleration obtained from Eq. (15). Shock response spectrum of a ground shock acceleration time history depends on the substructure resonance frequency. The shock response spectrum presumes that the mechanical shock pulse is applied as a common base input to a group of independent single-degree-of freedom systems. The shock response spectrum yields the peak response of each system with respect to the natural frequency of each system. Damping is typically fixed at a constant value, such as 5%, which is equivalent to an amplification factor of Q=10 (Tuma *et al*. 2011).

The absolute acceleration of the shock motion is defined by

$$\ddot{x}(t) = \omega\int_0^t a_g(\tau)\sin\omega(t-\tau)d\tau \tag{16}$$

The shock response spectrum is defined as the maximum $|\ddot{x}(t)|$ for each frequency

$$S_l = |\ddot{x}(t)|_{max} \tag{17}$$

Substituting Eq. (16) into Eq. (17), shock response spectrum with damping can be defined as

$$S_l = \left|\omega\int_0^t a_g(\tau)e^{-\xi\omega(t-\tau)}\sin\omega(t-\tau)d\tau\right|_{max} \tag{18}$$

where, a_g is base acceleration of a SDOF system as a function of time, and S_l is the spectral acceleration.

Shock response spectrum values depending on the frequency of total blast-induced ground motions (air blast and direct induced ground motions) are calculated by MATLAB (Mathworks 2012). The pull-down menu system in the BlastGM simplifies inputting the data, defining the analysis type, and showing the results. The program has the capability of transferring the resulting outputs as ANSYS txt file as well as plotting the shock response spectrum graphs due to blast-

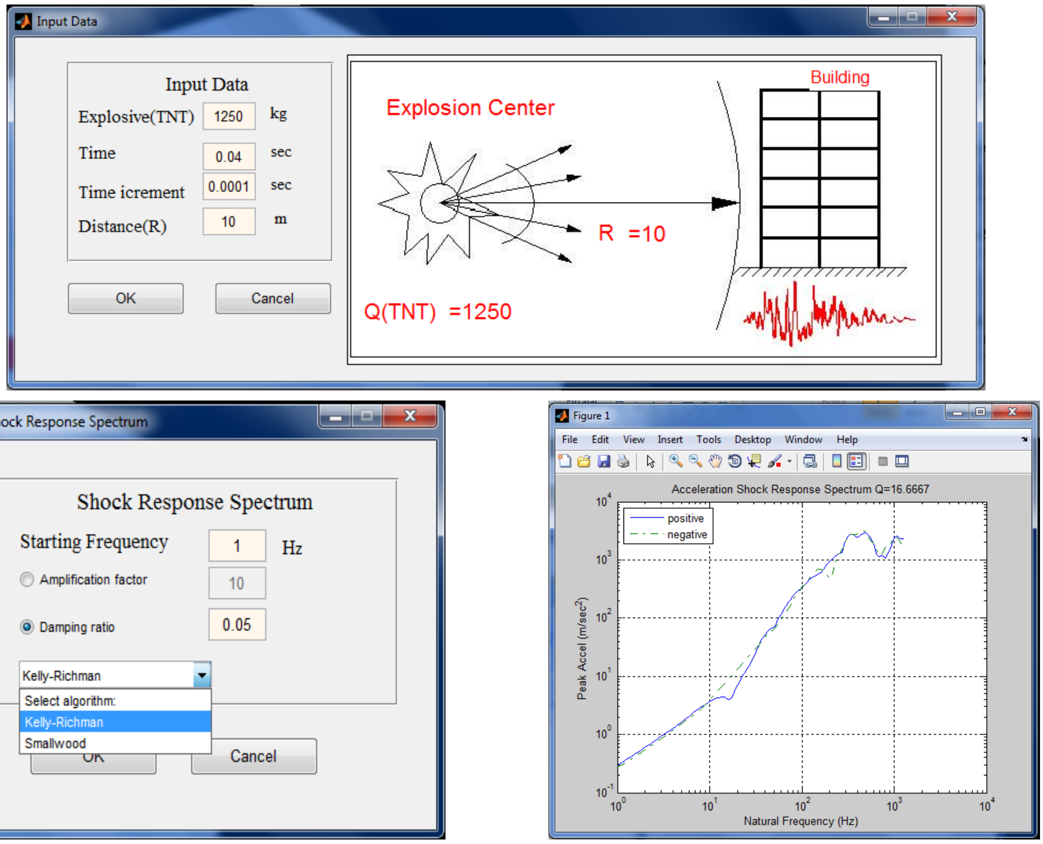

Fig. 4 Input data and shock spectrum results of the program

induced ground motions. Necessary output files are generated by the software to be utilized in ANSYS finite element program. The software has Turkish and English language options. Furthermore, SI and American Unit System (FPS) options are available in the software. Input data and analysis results parts of the program are presented in Fig. 4.

In order to estimate the effect of the total blast-induced ground motion on the dynamic response of a historical masonry bridge, three different charge weights and charge centers are used by employing the above mentioned software. The charge weights are chosen as 1250 kg, 1000 kg and 750 kg, with distances of 10 m, 15 m, and 20 m. The shock response spectrums obtained from the acceleration-time histories of each case are depicted in Figs. 5-6.

4. Numerical study

A masonry bridge, Kurt Bridge, located in Samsun, Turkey is selected for numerical calculations. Kurt Bridge shown in Fig. 7 is built on the Istavroz Brook which is drawing the borders of Vezirkopru and Havza, and connects Tahna Village (Havza) and Tekkekıran Village (Vezirkopru) to each other. The bridge stands over high two arches. The bridge has three pointed arch windows, one is located between the arches and the remaining two of them are located on the

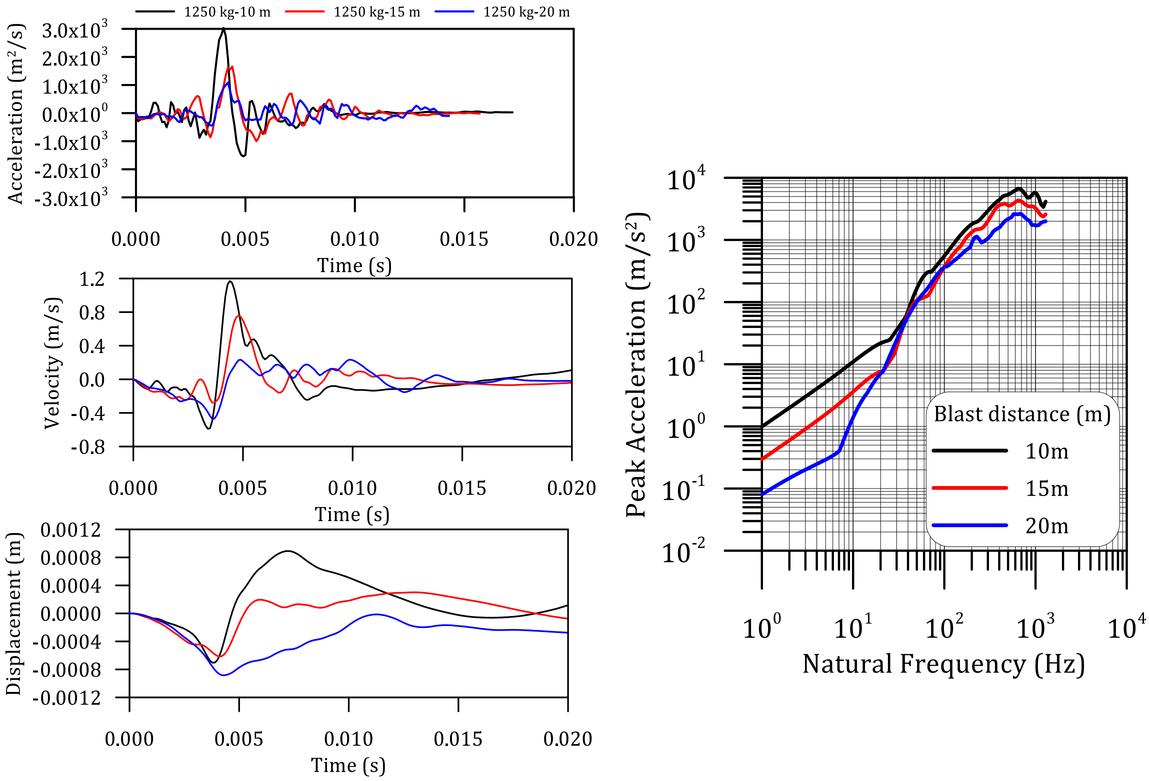

Fig. 5 Acceleration, velocity, displacement time histories and shock response spectrums for10 m, 15 m and 20 m blast distances under 1250 kg charge weight

sides of the arches. The rubble bonding system consisting of face stone and irregular stones is observed on the bridge. In the construction of the bridge, grave stones and architectural pieces belonging to Byzantine and Roman periods are also used as a gathered material. The architectural style and the bond system of the bridge are confirming to the 13th-14thcentury architecture (Samsun Guide 2010).

ANSYS (2013) finite element program is used to carry out the dynamic response analysis of the historical masonry bridge. In the analyses, the effect of the multi-point blast induced ground motion, the blast charge weight and the blast center on the dynamic response of the historical masonry bridge are investigated in detail. SOLID45 element is used for the three-dimensional modeling of the Kurt Bridge. This element is defined by eight nodes having three degrees of freedom at each node: translations in the nodal *x*, *y*, and *z* directions. Fig. 8 and Fig. 9 show the finite element model and cross-section of the Kurt Bridge. It is also seen in Fig. 8 that the variability of shock spectrum graphs according to different regions of the bridge due to 1250 kg of the charge weight and 10 meters of the blast distance.

Stone arch, side wall and timber block sections of the bridge are also taken into account in the finite element model. The material properties used for these sections are obtained from the successful studies performed on similar historical bridges (Frunzio *et al*. 2001, Diamanti *et al*. 2008, Ural 2005). The material properties obtained from the literature are given in Table 3 (Sevim *et al*. 2011).

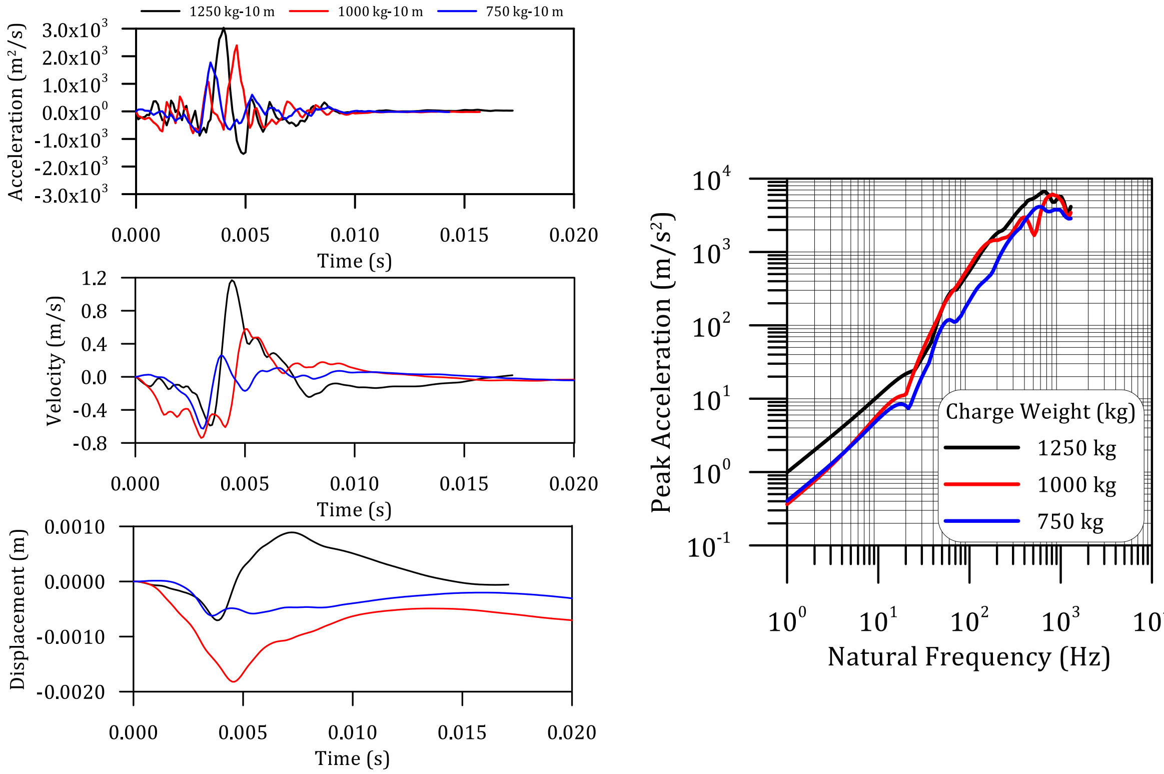

Fig. 6 Acceleration, velocity, displacement time histories and shock response spectrums due to 1250 kg, 1000 kg and 750 kg charge weights for 10 m blast distance

Table 3 Material properties of the bridge (Sevim *et al*. 2011)

Material	Modulus of Elasticity (N/m^2)	Poisson Ratio	Density (kg/cm^2)
Side walls	$2.5x10^9$	0.20	2464.4
Stone arches	$3.0x10^9$	0.25	2140.7
Filling	$1.5x10^9$	0.05	1600.0

Fig. 7 Photographs of Historical Kurt Bridge in Turkey

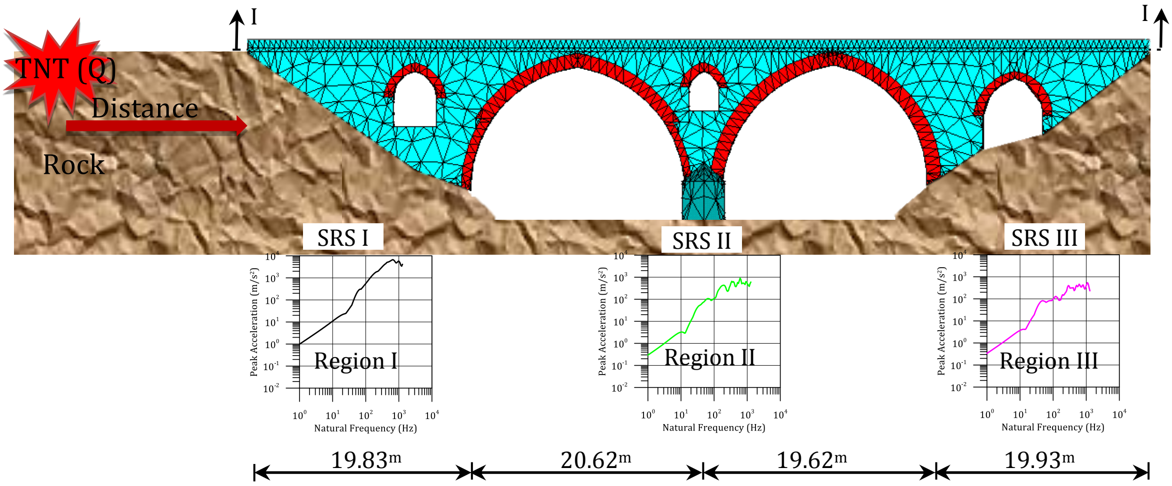

Fig. 8 Finite element model of the historical masonry bridge system

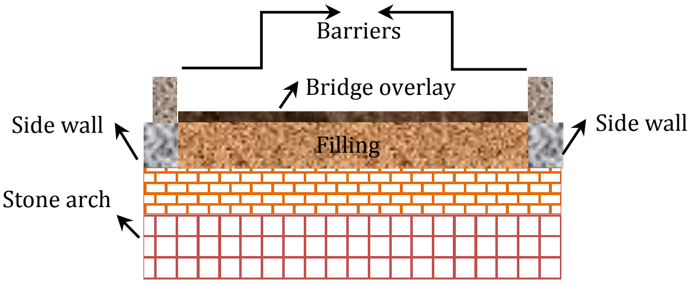

Fig. 9 Cross-section of the historical masonry bridge system

5. Numerical calculations

In this study, it is assumed that the historical masonry bridge located in a short distance from a quarry is continuously exposed to shock ground vibrations due to the quarry activities. This study explores the effect of multi-point blast-induced ground motion on the dynamic response of the considered historical masonry bridge for different charge weights and distances from the blast center by using the shock response spectrum method. Power spectral density functions used in the analyses are determined for the frequency range of 0.3 Hz-10 Hz (Wu and Hao 2007, Wu *et al*. 2005, Singh and Roy 2010).

a) Effect of the multi-point blast induced ground motion

Multi-point blast induced ground motion is applied to the historical masonry bridge model in the horizontal direction, as shown in Fig. 8. Shock response spectrums determined depending on the blast center distance from the structure and charge weight are applied to each support point of the model as SRS1, SRS2 and SRS3 in the direction of the blast induced ground motion. Due to the lack of suitable ground motion models for the spatial variability of multi-point blast induced

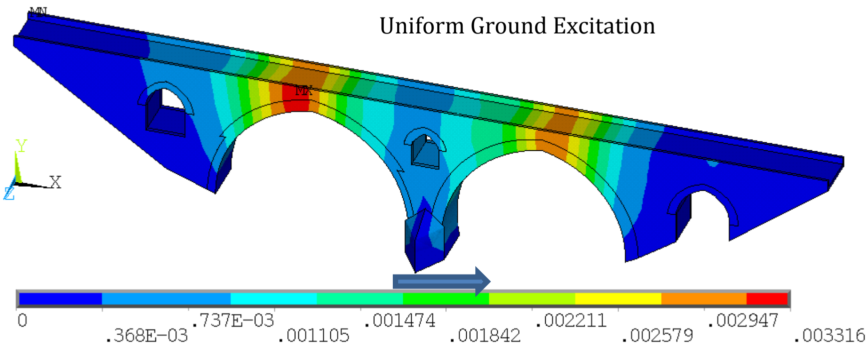

(a)

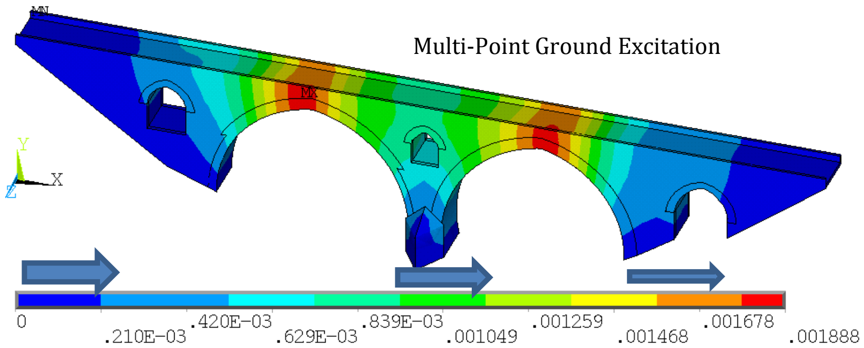

(b)

Fig. 10 Vertical spectral displacement response contours for (a) uniform and (b) multi-point ground motions

ground motions, the spatially varying ground motion components of wave passage and incoherent effects are not considered in this study for the blast-induced ground motions. In this part of this paper, responses obtained from the uniform and non-uniform (spatially varying) ground motions are compared with each other to determine the effect of the multi-point ground motion on the dynamic response of the historical masonry bridge. For this purpose, TNT charge weight and blast center distance from the structure are considered as 1250 kg and 10 m, respectively.

Figs.10-11 illustrate shaded image contours of spectral displacements (m) and Von Misses stresses (N/m^2) in the *X* direction of the Kurt Bridge when subjected to the uniform and multi-point blast-induced ground motions, respectively.

As Figs. 10-11 show, vertical displacements and Von Misses stresses in the longitudinal direction (X) determined from the multi-point blast induced ground motion are smaller than those of the blast induced uniform ground motion. Additionally, it can be observed that maximum vertical displacements take place at the top of big arches. As expected, maximum Von Misses stresses are observed at the parts closer to the base of the bridge.

b) Effect of the charge weight

In order to determine the effect of the charge weight on the dynamic response of the historical masonry bridge when subjected to the multi-point blast-induced ground motion, TNT charge weight is considered as 750 kg, 1000 kg and 1250 kg and the resulting vertical displacements and

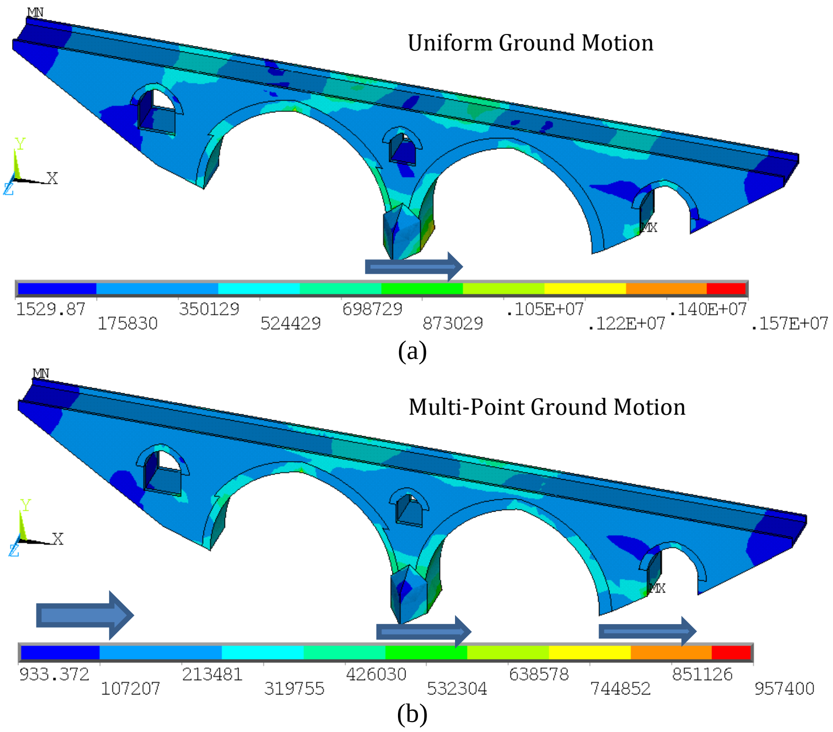

Fig. 11 Spectral stress response (Von Misses) contours for (a) uniform and (b) multi-point ground motions

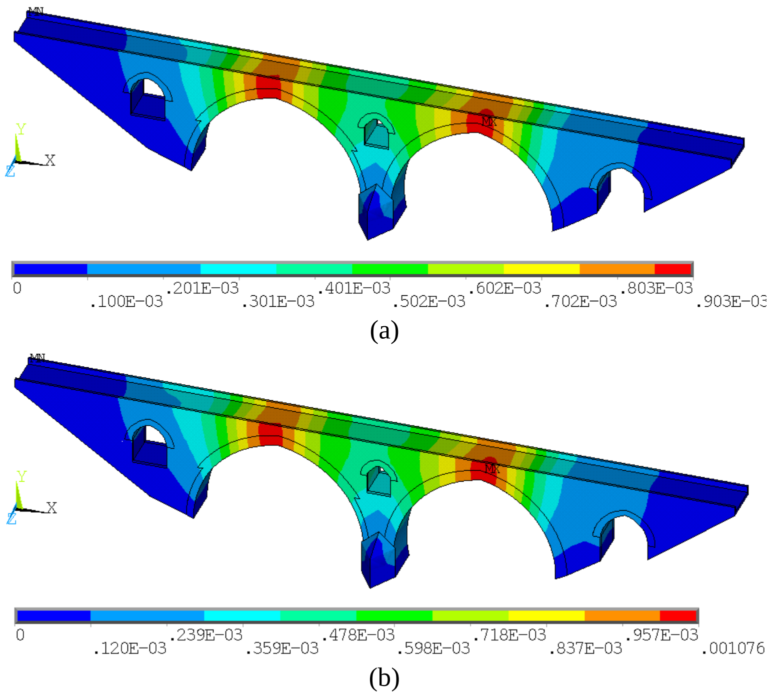

Fig. 12 Vertical spectral displacement response contours for the charge weight of (a) 750 kg, (b) 1000 kg and 1250 kg

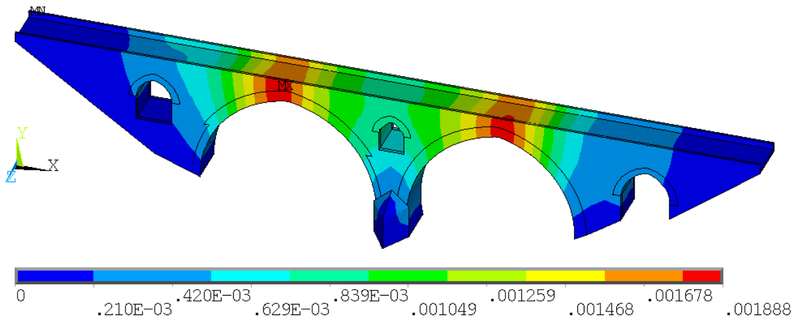

(c)

Fig. 12 Continued

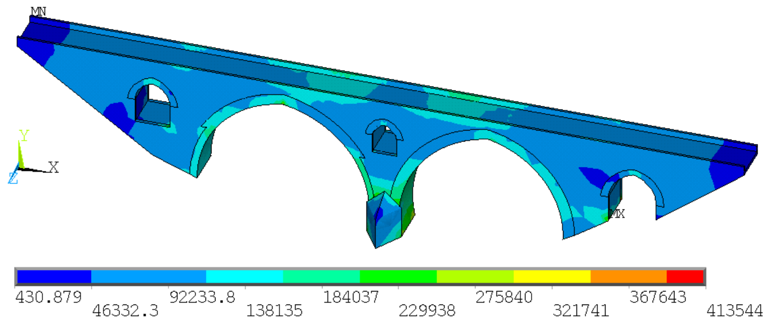

(a)

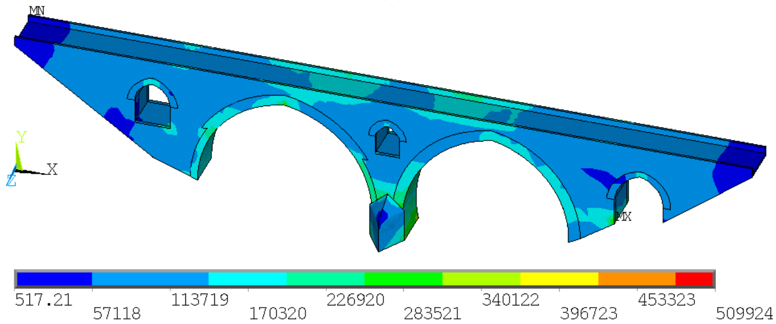

(b)

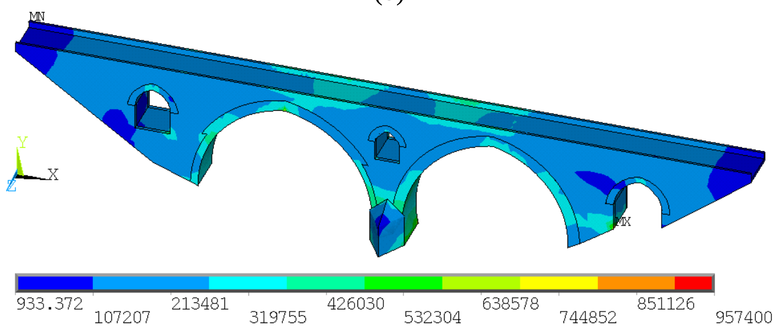

(c)

Fig. 13 Spectral stress response (Von Misses) contours for the charge weight of (a) 750 kg, (b) 1000 kg and 1250 kg

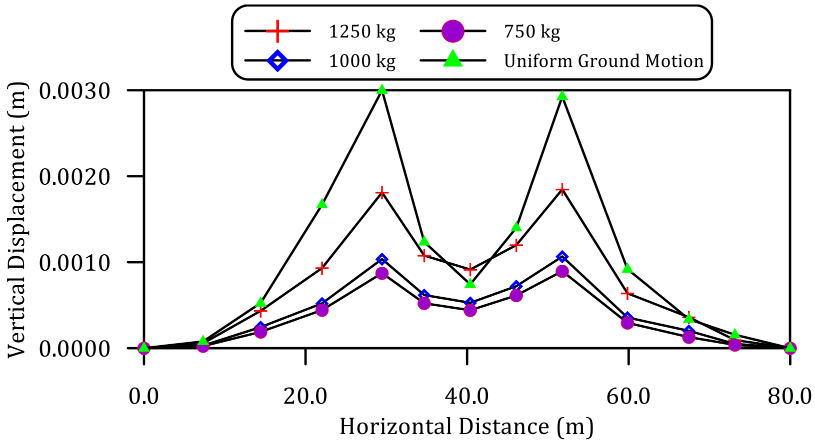

Fig. 14 Vertical spectral displacement response values at Section I-I for the charge weight of (a) 750 kg, (b) 1000 kg and 1250 kg

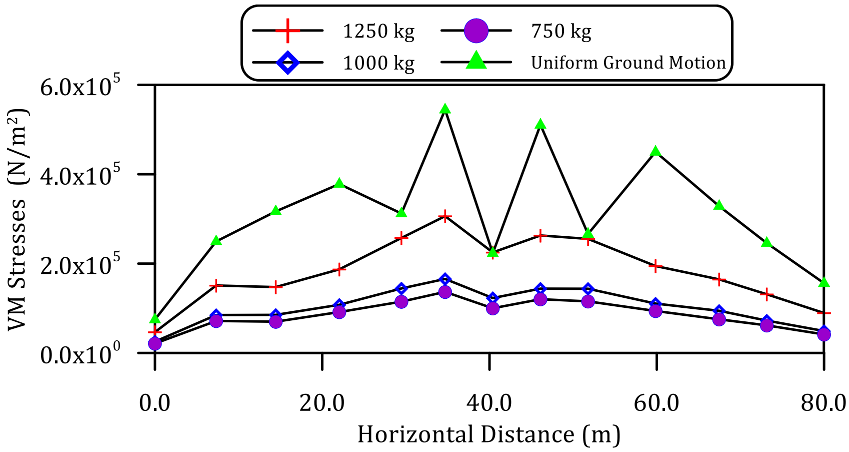

Fig. 15 Spectral stress response (Von Misses) values at Section I-I for the charge weight of (a) 750 kg, (b) 1000 kg and 1250 kg

the Von Misses (VM) stresses are shown in Figs. 12-15. Figs. 12-13 show the shaded image contours of the vertical displacements and Von Misses (VM) stresses determined for the considered blast charge weights, respectively.

In this section, the distance of the structure from the blast center is chosen as 10 m. As can be observed from the figures, the displacement and stress values change significantly depending on the amount of the charge weight (TNT). The displacement and stress values increase clearly depending on the increase in the amount of the charge weight. While the maximum displacements take place at the tops of the big arches, the maximum VM stresses take place at bridge sections close to the base of the bridge.

Vertical displacements and VM stresses determined at the top of the bridge along the longitudinal direction (Section I-I as shown in Fig. 8) are compared in Figs. 14-15, respectively. These figures also show that the structural responses increase with the increasing charge weights.

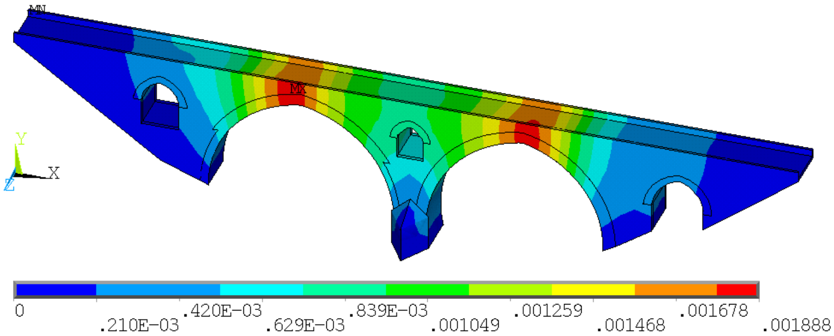

(a)

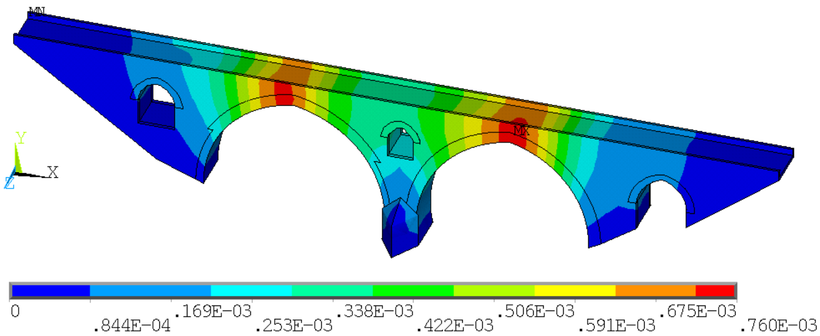

(b)

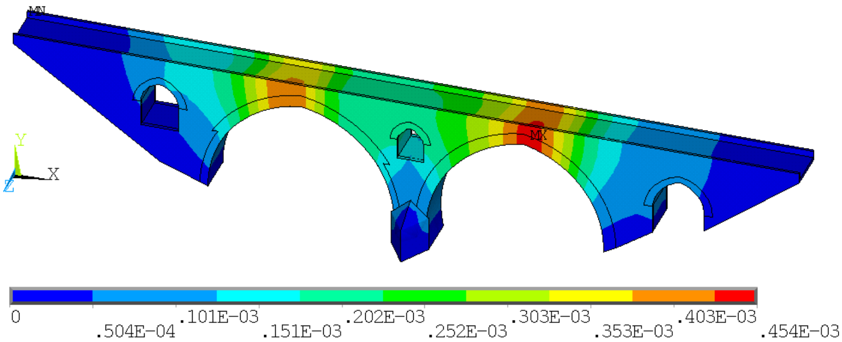

(c)

Fig. 16 Vertical spectral displacement response contours for (a) 10 m, (b) 15 m and 20 m blast distances

c) Effect of distance from the blast center

In this part of the study, the influence of the distance of the blast center from the structure is investigated to determine its effect on the dynamic response of the historical masonry bridge when subjected to the multi-point blast-induced ground motion. For this purpose, the distance of the blast center from the bridge is considered as 10, 15, 20 m for a parametric study. In the analyses herein, the TNT charge weight is considered as 1250 kg.

Fig. 16(a-c) and Fig. 18(a-c) show the shaded image contours of the vertical displacements and Von Misses (VM) stresses for the considered blast center distances, respectively. Vertical displacements and VM stresses determined at the top of the bridge along the longitudinal direction

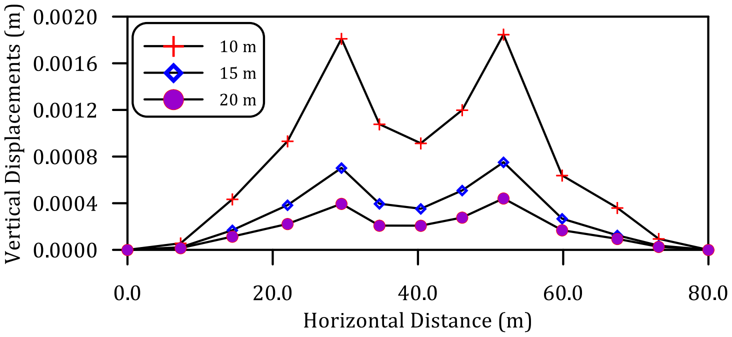

Fig. 17 Vertical spectral displacement response contoursat Section I-I for (a) 10 m, (b) 15 m and 20 m blast distances

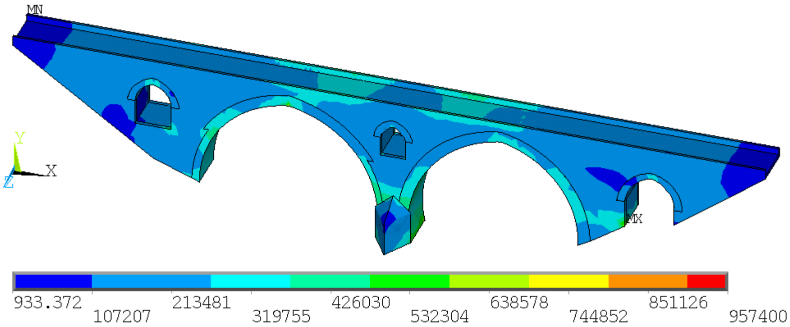

(a)

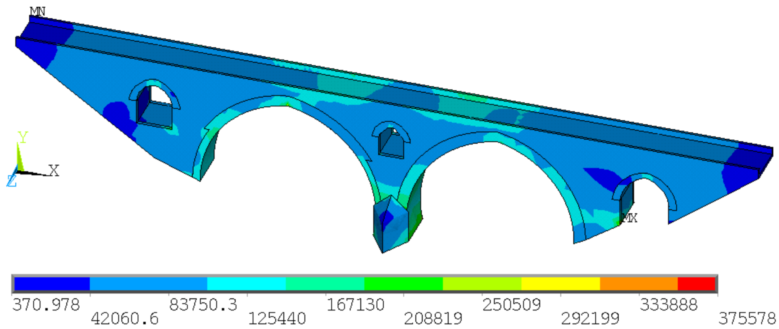

(b)

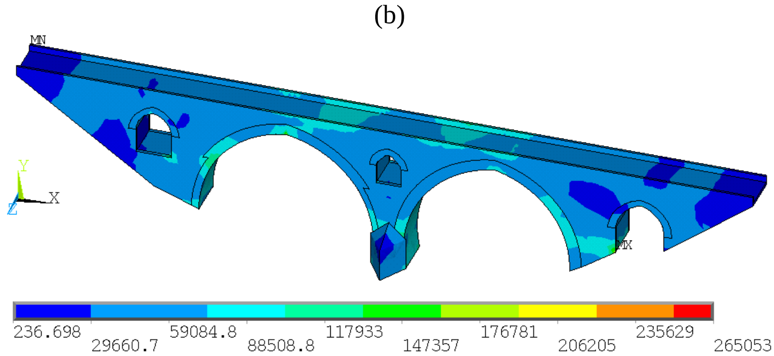

(c)

Fig. 18 Spectral stress response (Von Misses) contours for (a) 10 m, (b) 15 m and 20 m blast distances

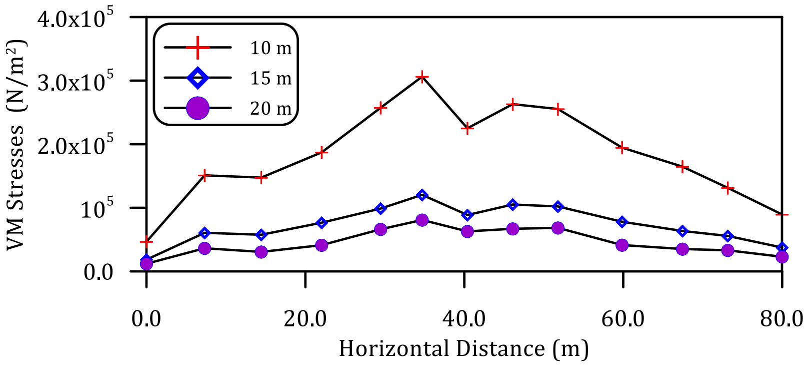

Fig. 19 Spectral stress responses (Von Misses) at Section I-I for (a) 10 m, (b) 15 m and 20 m blast distances

(Section I-I) are compared in Fig. 17 and Fig. 19, respectively. These figures clearly show that the displacement and stress values increase with decreasing distance between the structure and the blast center. While the maximum displacements take place at the tops of the big arches, the maximum VM stresses take place at bridge sections close to the base of the bridge as illustrated in Fig. 16 and Fig. 18, respectively. Finally, Fig. 17 and Fig. 19 also show that the vertical displacement and VM stress values at Section I-I increase with decreasing distance between the structure and the blast center.

6. Conclusions

The purpose of this study is to estimate the influence of the multi-point blast-induced ground motions on the dynamic response of historical masonry bridges. For this purpose, a historical masonry Kurt Bridge located in Turkey is selected and multi-point response spectrum method is used to determine the dynamic behavior of this bridge. For this purpose, the finite element program ANSYS software is used for the response calculations. To determine the effect of the multi-point blast induced ground motion on the bridge model, a parametric study is conducted depending on different blast charge weights and blast distances.

The results of the analyses show that larger response values are obtained for uniform ground motion when compared with the responses obtained from the multi-point blast-induced ground motion. Significant differences are observed between the uniform and multi-point blast-induced ground motions. However, it should be emphasized that the multi-point blast-induced ground motion significantly changes the dynamic response of the bridge.

Additionally, the resulting bridge responses obtained for different blast charge weights and blast charge distances show that increasing the blast charge weight and decreasing the blast charge distance results larger response values. While the stress accumulations take place at the bridge parts closer to the base of the bridge, maximum vertical displacements take place at the top of the big arches.

This study reveals that neglecting the blast-induced ground motion effect on historical masonry bridges might cause underestimation of the structural damage under certain circumstances. The results of the parametric study underline the remarkable effect of the surface blast-induced ground motions on the dynamic response of historical masonry bridges. Therefore, multi-point response spectrum method should be considered for the safe and economic design of historical masonry bridges when subjected to the blast induced ground motions.

Acknowledgements

This paper is supported by the Scientific and Technological Research Council of Turkey (TUBITAK) within International Research Fellowship Program and Branch Directorate of Historic Bridges of Turkey, Ankara.

References

Amin, M. and Ang, A.H.S. (1968), "A non-stationary stochastic model of earthquake motion", *J. Eng. Mech. Div*., **94**, 559-583.

ANSYS 14 (2013), Swanson Analysis System, US.

Bayraktar, A., Altunısık, A.C., Turker, T. and Sevim, B. (2007), "The model updating of historical masonry bridges using operational modal analysis method", *Proceedings of the 1st National Conference Reinforcement and Transfer into the Future of Historical Structures*, Ankara, Turkey, Chamber of Civil Engineering, September.

Bhatti, A.Q. (2009), "Seismic vulnerability of historical arch type bridge structures in Italy", Master's Thesis, Advanced Masters in Structural Analysis of Monuments and Historical Constructions.

Bolotin, V.V. (1960), "Statistical theory of the seismic design of structures", *Proceedings of the 2nd World Conference on Earthquake Engineering*, Tokyo.

Diamanti, N., Giannopoulos, A. and Forde, M.C. (2008), "Numerical modelling and experimental verification of GPR to investigate ring separation in brick masonry arch bridges", *NDT E Int*., **41**(5), 354-363.

Dowding, C.H. (1996), *Construction Vibrations*, New Jersey, Prentice-Hall.

Frunzio, G., Monaco, M. and Gesualdo, A. (2001), "3D FEM analysis of a roman arch bridge", *Histori. Construct*., 591-598.

Gonen, H., Dogan, M., Karacasu, M., Ozbasaran, H. and Gokdemir, H. (2013), "Structural failures in refrofit historical murat masonry arch bridge", *Eng. Fail. Anal*., **35**, 334-342.

Gupta, A.K. (1992), *Response Spectrum Method in Seismic Analysis and Design of Structures*, CRC Press, Boca Raton, Florida.

Hacıefendioğlu, K. and Alpaslan, E. (2014), "Stochastically simulated blast-induced ground motion effects on nonlinear response of an industrial masonry chimney", *Stoc. Environ. Res. Risk Assess*., **28**, 415-427

Hacıefendioğlu, K., Kartal, M.E. and Karaca, Z. (2013), "The effect of seasonally frozen soil on stochastic response of elevated water tank under random excitation", *Stoc. Environ. Res. Risk Assess*., **27**(4), 807-818.

Hacıefendioğlu, K., Soyluk, K. and Birinci, F. (2012), "Numerical investigation of stochastic response of an elevated water tank to random underground blast loading", *Stoc. Environ. Res. Risk Assess*., **26**(4), 599-607.

Hao, H. (1989), "Effect of spatial variation of ground motions on large multiply-supported structures", Report No. EERC-89/6, Earthquake, Engineering Research Center, University of California at Berkeley.

Hao, H. and Wu, C. (2005), "Numerical study of characteristics of underground blast induced surface ground motion and their effect on above-ground structures Part II: effects on structural responses", *Soil Dyn. Earthq. Eng*., **25**, 39-53

Hao, H., Wu, Y.K., Ma, G.W. and Zhou, Y.X. (2001), "Characteristics of surface ground motions induced by blast in jointed rock mass", *Soil. Dyn. Earthq. Eng*., **21**, 85-98.

Harichandran, R.S., Hawwari, A. and Sweidan, B.N. (1996), “Response of long-span bridges to spatially varying ground motion”, *J. Struct. Eng*., **122**, 476-84.
Harichandran, R.S. and Wang, W. (1990), “Response of indeterminate two-span beam to spatially varying seismic excitation”, *Earthq. Eng. Struct. Dyn*., **19**(2), 173-187.
Hiroaki, T. and Charles, D.H. (1984), “One and two support models for blast response”, *J. Geotech. Eng*., **110**(6), 675-683
Jennings, P.C., Housner, G.W. and Tsai, N.C. (1969), “Simulated earth quake motions for design purposes”, *Proceedings of the 4th World Conferences on EarthquakeEngineering*, **1**, 145-160.
Kanai, K. (1957), “Semi-empirical formula for the seismic characteristics of the ground”, *Bulletin of the Earthquake Research Institute*, University of Tokyo, **35**, 307-325.
Kanasewich, E.R. (1981), *Time Sequence Analysis in Geophysics*, The University of Alberta Press, Edmonton
Köksal, O. (2013), “Dynamic analysis of elevated steel water tank subjected to blast induced ground motion”, Master’s thesis in Civil Engineering, Institute of Science, Ondokuz Mayis University, Turkey.
Lu, Y. and Wang, Z. (2006), “Characterization of structural effects from above-ground explosion using coupled numerical simulation”, *Comput. Struct*., **84**, 1729-1742
Ma, H.J., Quek, S.T. and Ang, K.K. (2004), “Soil-structure interaction effect from blast-induced horizontal and vertical ground vibration”, *Eng. Struct*., **26**, 1661-1675
Mathworks Inc. MATLAB (2012), *The Language of Technical Computing*, Natick, Massachusetts, USA
Mclaughlin, K., Johnson, L. and McEvily, T. (1983), “Two-dimensional array measurements of near sources ground accelerations”, *Bull. Seismol. Soc. Am*., **73**, 349-76.
Pelà, L., Aprile, A. and Benedetti, A. (2009), “Seismic assessment of masonry arch bridges”, *Eng. Struct*., **31**, 1777-1788.
Regulatory Guide (1976), Regulatory Guide 1.92, U.S. Nuclear Regulatory Commission, Revision 1. February.
Reinke, R.E. and Stump, B.W. (1988), “Stochastic geologic effects on near-field ground motions in alluvium”, *Bull. Seismol. Soc. Am*., **78**, 1037-1058.
Ruiz, P. and Penzien, J. (1969), “PSEQN: Artificial generation of earthquake accelerograms”, Earthquake Engineering Research Center, Report No EERC 69-3, University of California, Berkeley.
Samsun Guide (2010), *Ministry of Culture and Tourism*, Yeşilırmak River Basin Development Union.
Sayın, E., Karaton, M., Yön, B. and Calayır, Y. (2011), “Tarihi Uzunok Köprüsünün Yapı Zemin Etkileşimi Dikkate Alınarak Doğrusal Olmayan Dinamik Analizi, 1”, Türkiye Deprem Mühendisliği ve Sismoloji Konferansı 11-14 Ekim 2011-ODTÜ -ANKARA.
Sevim, B., Bayraktar, A., Altunişik, A.C., Atamtürktür, S. and Birinci, F. (2011), “Finite element model calibration effects on the earthquake response of masonry arch bridges”, *Finite Elem. Anal. Des*., **47**, 621-634.
Singh, P.K. and Roy, M.P. (2010), “Damage to surface structures due to blast vibration”, *Int. J. Rock Mech. Min. Sci*., **47**, 949-961.
Tajimi, H. (1960), “A statistical method for determining the maximum response of a building structure during an earthquake”, *Proceedings of the 2nd World Conf. Earthquake Engineering*, Tokyo and Kyoto, Japan.
Todo, H. and Dowding, C. (1984), “One and two support models for blast response”, *J. Geotech. Eng*., **110**(6), 675-683.
Toker, S. and Unay, A.I. (2004), “Mathematical modelling and finite element analysis of masonry arch bridges”, Journal of Science of Gazi University, 17(2), 129-139.
Tuma, J., Babiuch, M. and Koci, P. (2011), “Calculation of a Shock Response Spectra”, *Acta Montanistica Slovaca*, **1**, 66-73.
UFC (Unified Facilities Criteria) (2008), “Structures to Resist the Effects of Accidental Explosions”, UFC 3-340-02, Department of Defense, US Army Corps of Engineers, Naval Facilities Engineering Command, Air Force Civil Engineer Support Agency, United States of America
Ural, A. (2005), “Finite element analysis of historical arch bridge”, *International Earthquake Symposium*

Kocaeli, Kocaeli, Turkey, March.
Ural, A., Oruç, S.¸Doğangün, A. and Tuluk, Ö.İ. (2008), "Turkish historical arch bridges and their deteriorations and failures", *Eng. Fail. Anal*., **15**, 43-53.
Url-1 (2014), "Protection of Turkish Cultural Heritage Abroad and Prevention of Illegal Trafficking of Turkish Cultural Heritage", http://www.mfa.gov.tr/protection-of-turkish-cultural-heritage-abroad-and-prevention-of-illegal-trafficking-of-turkish-cultural-heritage.en.mfa.
Wu, C. and Hao, H. (2004), "Modeling of simultaneous ground shock and airblast pressure on nearby structures from surface explosions", *Int. J. Impact Eng*., **31**, 699-717.
Wu, C. and Hao, H. (2005), "Numerical study of characteristics of underground blast induced surface ground motion and their effect on above-ground structures Part I: ground motion characteristics", *Soil Dyn. Earthq. Eng*., **25**, 27-38.
Wu, C. and Hao, H. (2007), "Numerical simulation of structural response and damage to simultaneous ground shock and airblast loads", *Int. J. Impact Eng*., **34**, 556-572.
Wu, C., Hao, H. and Lu, Y. (2005), "Dynamic response and damage analysis of masonry structures and masonry infilled RC frames to blast ground motion", *Eng. Struct*., **27**, 323-333.

CC